Incorporation of Cloud-Scale and Mesoscale Downdrafts into a Cumulus Parameterization: Results of One- and Three-Dimensional Integrations

JOHN MOLINARI AND TOM CORSETTI*

Department of Atmospheric Science, State University of New York at Albany, Albany, NY 12222

(Manuscript received 18 June 1984, in final form 2 January 1985)

ABSTRACT

Cumulus and mesoscale downdrafts are incorporated into the cumulus parameterization of Kuo. Convection is driven by grid-scale moisture supply, and distributed vertically by temperature and specific humidity differences between the environment and an idealized cloud. The moisture supply is defined to minimize the problem of lag between instantaneous moisture accession and rainfall. Downdrafts are added to the idealized cloud profile by determining a weighted mean of the equivalent potential temperatures (θ_e) for cumulus updrafts, saturated cumulus downdrafts, and unsaturated mesoscale downdrafts, and by extracting the cloud temperature and specific humidity iteratively from the mean θ_e. The θ_e values are weighted by the mean vertical eddy flux convergence of moist static energy by each component.

The addition of downdrafts sharply increases the rate of stabilization of the grid scale by the Kuo approach. Stabilization characteristics are also shown to depend upon precipitation efficiency, strength of grid-scale forcing, downdraft relative humidity, downdraft weighting, and intensity of surface fluxes.

The approach was tested in a real-data, three-dimensional primitive equation prediction of a mesoscale convective complex (MCC) on a 1° latitude/longitude mesh. Prediction of total rain volume was most accurate when downdrafts were included. Without downdrafts, a feedback instability occurred at the MCC center and rainfall was greatly overestimated. When convective heating was omitted, so that rainfall could be produced only after grid-scale saturation, predicted rainfall was less than 10% of that observed and the MCC decayed. Difference vectors between the full and no convection integrations showed strong outflow developing in the upper troposphere, evolving to a large anticyclonic eddy following the MCC by hour 12 of the forecast. Corresponding inflow and a weak cyclonic eddy developed at low levels. Influence of the MCC spread rapidly over several hundred kilometers through this divergent flow. The results indicate, not surprisingly, that maintenance of the MCC depends critically on the presence of cumulus convection. The failure of the explicit (nonparameterized) approach suggests that cumulus parameterization is necessary for realistic prediction of convective systems in meso-α scale models.

In the integration with downdrafts incorporated, a life cycle behavior occurred in the heavy rainfall region. The level of maximum upward motion shifted from middle to upper levels over several hours, and downward motion developed at the lowest levels. The apparent heat source was initially positive at all levels, then became negative in the lower troposphere and more strongly positive aloft. Stratiform precipitation fell from saturated upper levels for a brief period after convection ceased. This life cycle behavior, which contains several aspects of that observed, took place only when cumulus and mesoscale downdrafts were incorporated.

1. Introduction

The parameterization of vertical heat and moisture transports by cumulus convection has remained a major unsolved problem in numerical weather prediction. The role of deep precipitating cumulus clouds in stabilizing the large scale, chiefly through low-level cooling by nearly saturated cloud-scale downdrafts, has long been recognized. Analyses from GATE and other data collection efforts, however, have revealed that deep convection is accompanied by unsaturated downdrafts on a scale larger than individual cumulus clouds (Zipser, 1969; Houze, 1982). These mesoscale downdrafts are driven by cooling due to melting and evaporation of stratiform precipitation (Brown, 1979; Leary and Houze, 1979), which is produced both in upper tropospheric anvil clouds and by ejection from adjacent cumulus updrafts (Churchill and Houze, 1984). The unsaturated downdrafts may exist for 100 km or more in the wake of a propagating system, and become increasingly important over 6–12 hours as the convective cloud cluster undergoes a life cycle (Houze, 1982). They play a significant thermodynamic role by cooling and moistening the lower troposphere, while active anvil updrafts produce warming and drying above the freezing level (Johnson and Young, 1983; Houze, 1982). Hartman *et al.* (1984) found that a "mature cluster" heating profile, which included mesoscale influences, more accurately reproduced the tropical Walker Circulation in a linear steady-state

* Current affiliation: Sigma Data Corporation, Greenbelt, MD 20771.

model than an isolated cumulonimbus heating profile. The authors suggested that the mesoscale cluster profile may represent the dominant mode of diabatic heating in the tropics. The evidence indicates that the thermodynamic effects of mesoscale circulations cannot be neglected.

In meso-α scale numerical models (grid spacing 50–250 km), the presence of these mesoscale processes greatly complicates the cumulus parameterization problem. Initially the unsaturated downdrafts accompany active cumulus scale updrafts and downdrafts, i.e., occur at the same grid point, and thus must be parameterized. As the convective cluster matures, however, the mesoscale downdrafts cover an increasing percentage of the area. Eventually, the convective updrafts stop and only the mesoscale circulation remains at the grid point (e.g., Johnson and Kriete, 1982), or the convectively active region propagates to an adjacent grid point, leaving a mesoscale downdraft in its wake. In either case, the unsaturated downdraft becomes (at the original point) an explicit grid scale phenomenon, unaccompanied by the convective scale, and is no longer parameterized. The meso-α scale modeler must simulate (a) the vertical distributions of heat and moisture sources due to subgrid scale convection; (b) their time variation over the life cycle of the system, as mesoscale downdrafts increase in percent areal coverage; and (c) the grid scale residue left behind.

In the current work, a method is proposed based on the work of Kuo (1974) which incorporates, following the suggestion of Molinari (1982b), a parametric representation of cumulus and mesoscale downdrafts into the vertical distribution functions. Only the thermodynamic effects of cumulus convection will be addressed; observational aspects of cumulus momentum transport are still too poorly understood to develop a parameterized approach. In the following sections, the properties of the Kuo approach are examined, the addition of downdrafts described, and the stabilization characteristics presented. The proposed approach is tested in a three-dimensional primitive equation prediction of a mesoscale convective complex, and is shown to produce a life-cycle behavior with many similarities to that observed.

2. Review of Kuo's approach

a. Definition of the moisture supply

The fundamental assumption of Kuo's approach relates intensity of convective forcing to the instantaneous rate at which moisture is supplied to the grid point. As a consequence, definition of the moisture supply takes on considerable importance. Kuo (1965) used the sum of the three-dimensional grid-scale moisture convergence and the surface evaporation. The basis for the Kuo approach was called into question when Betts (1978) and Frank (1979) noted a lag of several hours between moisture convergence and precipitation. Kanamitsu (1975) and Krishnamurti *et al.* (1976) used only vertical advection to define the moisture supply (omission of subscripts indicates grid scale variables):

$$I = -\frac{1}{g}\int_{p_t}^{p_b}\left(\omega\frac{\partial q}{\partial p}\right)dp. \tag{1}$$

Recently, Y. H. Kuo (1983) compared the two definitions using high-resolution SESAME data. He found that although vertically integrated moisture convergence lagged precipitation by increasing amounts with increasing horizontal scale, the quantity in (1) contained no lag on any scale, even 750 × 750 km. These results suggest that Kuo's (1965) assumption of rainfall proportional to the instantaneous rate of moisture supply at a grid point is realistic, as long as moisture supply is defined by the vertically integrated vertical moisture advection.

As a consequence of (1), horizontal advection of moisture and surface evaporation do not contribute directly to convection, but act only to change the grid scale. These processes do enter the convective moisture source the subsequent time step, but only to the extent that they change the grid-scale $\partial q/\partial p$. In (1), $I > 0$ indicates the active lifting of moisture and thus the presence of a destabilizing mechanism. It is physically more reasonable to initiate convection using $I > 0$ in (1) than simply in the presence of positive horizontal advection or surface evaporation alone, without significant upward motion. Support for this view is provided by Houze and Betts (1981), who review several papers that show the high correlation between mean vertical motion and rainfall in GATE. Y. H. Kuo's findings indicate that lag due to liquid water storage (e.g., see Betts, 1978), which cannot be addressed by this approach, may not be a serious problem in deep convective situations. Equation (1) is adopted in this study.

b. Kuo-Kanamitsu-Krishnamurti approach

Neglecting nonconvective heating and horizontal advection, equations for potential temperature and specific humidity changes in the Kuo approach can be written (Kanamitsu, 1975; Krishnamurti *et al.*, 1976) as

$$\frac{\partial\theta}{\partial t} = -\omega\frac{\partial\theta}{\partial p} + a_\theta\left\{\frac{\theta_c - \theta}{\Delta\tau} + \omega\frac{\partial\theta}{\partial p}\right\}, \tag{2}$$

$$\frac{\partial q}{\partial t} = a_q\left(\frac{q_c - q}{\Delta\tau}\right), \tag{3}$$

where

$$a_\theta = \frac{(1-b)I}{Q_\theta} \tag{4}$$

is the fractional approach of the grid scale to the limiting state potential temperature θ_c in time $\Delta\tau$, and

$$a_q = \frac{bI}{Q_q} \tag{5}$$

is the fractional approach to q_c. The b parameter (Kuo, 1974), which is the fraction of moisture supply I that increases storage ($1 - b$ is the grid-scale precipitation efficiency), is discussed in Section 2c, and Q_θ and Q_q are defined in Appendix A. No loss of generality occurs by considering vertical advection only because, as noted earlier, horizontal advection and surface fluxes do not interact directly with the convection. The origin of (2)–(3) and energy and moisture conservation in the approach are shown in Appendix A.

A generalized Kuo scheme can be written from (2)–(5), using (A7) and (A8) of Appendix A, as

$$\frac{T}{\theta}\frac{\partial\theta}{\partial t} = -\omega\frac{T}{\theta}\frac{\partial\theta}{\partial p} + g\frac{L}{c_p}(1-b)I\frac{\alpha}{\langle\alpha\rangle}, \tag{6}$$

$$\frac{\partial q}{\partial t} = gbI\frac{\beta}{\langle\beta\rangle}, \tag{7}$$

where

$$\alpha = \frac{T}{\theta}\left(\frac{\theta_c - \theta}{\Delta\tau} + \omega\frac{\partial\theta}{\partial p}\right), \tag{8}$$

$$\beta = \frac{q_c - q}{\Delta\tau}, \tag{9}$$

$$\langle\ \rangle = \int_{p_t}^{p_b}(\ )dp.$$

Equations (6)–(7) show that convective heating and moistening in the Kuo-Kanamitsu-Krishnamurti approach are forced by moisture supply I, partitioned by the b parameter, and vertically distributed by the functions α and β. With vertical distributions given by (8)–(9), the grid column is moved toward the limiting state represented by θ_c and q_c at a rate which depends upon many factors, including the strength of forcing, the presence of downdrafts, and the moisture partitioning, as discussed in Section 4. In this manner the Kuo approach, rather than a pure mixing approach, can be viewed as a variable-rate, time-dependent form of convective adjustment.

Because the integral constraints on energy and moisture (Eq. A9 and A14) hold for any values of θ_c, q_c, and b, a numerical modeller is free to adjust these variables to incorporate additional physical effects into the adjustment process. The addition of cumulus and mesoscale downdrafts to the limiting state will be described in Section 3.

The vertical distribution functions α and β appear arbitrary in (6)–(7). In reality, however, they are subject to an additional constraint (Kanamitsu, 1975): as a layer reaches moist neutrality ($T \to T_c$, $q \to q_c$), the local changes of θ and q must vanish, because no change occurs in either variable due to rising motion in a moist neutral layer. This condition must hold to insure a smooth transition between conditionally unstable and neutral lapse rates. The current approach satisfies this constraint as long as (a) $b \to 0$ as $T \to T_c$ and $q \to q_c$, and (b) T_c and q_c approach a moist adiabat as saturation is reached (see Appendix A). The inclusion of downdrafts will be made to satisfy these added constraints.

c. *Definition of the moisture partitioning*

The choice of the moisture partitioning parameter is critical in the Kuo-Kanamitsu-Krishnamurti approach, for two reasons:

(i) It determines whether net warming or cooling of the column occurs (e.g., Molinari, 1982b), and thus partly controls the feedback of the convection on the intensity of the grid-scale vertical circulation.

(ii) In a diagnostic or semi-prognostic framework, the precipitation rate for a given moisture supply depends entirely on the moisture partitioning, regardless of the idealized cloud model used to get θ_c and q_c. In a prognostic framework, the vertical distribution of heating also becomes a major factor, as will be shown in the one and three-dimensional integrations.

Molinari (1982b) proposed the following closure for b, which insured that temperature and specific humidity approach their limiting state at the same rate:

$$\int_{p_t}^{p_b}(T_c - T)dp \Big/ \int_{p_t}^{p_b}\frac{\partial T}{\partial t}dp = \int_{p_t}^{p_b}(q_c - q)dp \Big/ \int_{p_t}^{p_b}\frac{\partial q}{\partial t}dp. \tag{10}$$

The time change terms in the denominator were determined from (2)–(3). Equation (10) leads to (adiabatic cooling A is defined by Appendix Eq. A10)

$$b = \frac{A + I}{I}\left\{\frac{Q_q}{Q_q + Q_\theta + A}\right\}. \tag{11}$$

Typically $b \sim 0.1$ with this approach, which Molinari (1982b) found to be the only one of four tested to produce a uniform approach to moist neutrality in both θ and q. Equation (11) fails to do so, however, when downdrafts are included in the limiting state. The difficulty relates to the change of sign of $T_c - T$, which can make $\int_{p_t}^{p_b}(T_c - T)dp = 0$ when $\int_{p_t}^{p_b}|T_c - T|dp$ is far from zero. No alteration of (10) could be found which produced a unique solution for b, and the procedure was abandoned.

Several alternative formulations for b have been proposed (Kanamitsu, 1975; Anthes, 1977; Krishna-

murti *et al.*, 1980; 1983). In the current study, b is defined following Fritsch and Chappell (1980a), who derived a functional form for precipitation efficiency $1 - b$ versus vertical shear. Their form was chosen because it is supported by the greatest number of independent observational studies. It should be noted, however, that most formulations for b give values between 0.1 and 0.3 (except Anthes, 1977, which is generally larger). The sensitivity of results to the b parameter is examined in Section 4.

The b parameter is redefined from the vertical shear dependent value under one circumstance, when $a_\theta > 1$. In such a situation, $(1 - b)I > Q_\theta$, which indicates that moisture available for condensation heating is greater than that needed to form a cloud in time $\Delta\tau$. This can be considered an instability in the approach, because a_θ can be arbitrarily large, and the limiting profile can be reached in a time much less than $\Delta\tau$. In order to prevent the instability, b is redefined to make $a_\theta = 1$, i.e., from (4),

$$b = \frac{I - Q_\theta}{I} \quad \text{if} \quad a_\theta > 1. \tag{12}$$

This procedure has the additional benefit that as $T \rightarrow T_c$ and $q \rightarrow q_c$, it can be seen from (1), (A7), and (A16) that $b \rightarrow 0$, and the necessary condition on b for the transition to a neutral state is satisfied. The adjustment to b thus serves two purposes: to prevent a potential instability in the approach, and to promote a smooth transition to a neutral state. When a_θ reaches and remains at unity (and only then), $\Delta\tau$ becomes the time scale for stabilization of the grid column; this occurs under strong forcing or when the entraining updraft has nearly zero buoyancy.

3. Addition of downdrafts

Three components make up the final T_c and q_c profiles: cumulus-scale updrafts, cumulus-scale downdrafts, and mesoscale downdrafts. Values of θ_e at each level for the three components (θ_{eu}, θ_{ed} and θ_{em}, respectively) are determined, a weighted mean θ_e and q calculated (θ_{ec}, q_c), and T_c extracted iteratively. Above the downdraft layer, only θ_{eu} is used; mesoscale updrafts are not explicitly included. It will be shown in the three-dimensional results that despite this limitation, saturated upper tropospheric ascent develops on the grid scale, for reasons to be discussed later. The procedure for incorporating downdrafts is as follows (cloud base and cloud top definitions follow Molinari, 1982b):

(i) The entraining updraft is computed similar to Fritsch and Chappell, (1980a):

$$\theta_{eu}(K+1) = \left(\frac{1}{1 + E\Delta p}\right)\theta_{eu}(k) + \left(\frac{E\Delta p}{1 + E\Delta p}\right)\tilde{\theta}_e(k), \tag{13}$$

where $E\Delta p$ is equivalent to $\Delta M_u/M$ in the Fritsch-Chappell approach, Δp is layer thickness, $\tilde{\theta}_e$ is the mean environmental θ_e over Δp, and

$$E = \gamma/H$$

is the entrainment, with H the cloud depth in mb. Because the Kuo approach models deep clouds, H is chosen as the deepest possible cloud and $\gamma = 1$, rather than the iterative approach for E used by Molinari (1982b). At cloud base, $\theta_{eu} = \tilde{\theta}_{es}$, and a simple ice phase parameterization is used following Fritsch and Chappell (1980a).

(ii) Also following Fritsch and Chappell, $\theta_{ed} = \frac{1}{2}(\theta_{eu} + \tilde{\theta}_e)$ at cumulus downdraft top, which is defined as the first layer at or below 550 mb in which $\theta_{ed} < \tilde{\theta}_{es}$, with the additional constraint that it be at least 100 mb below cloud top. The entraining downdraft θ_e is computed analogously to (13). Following Johnson (1976), the cumulus downdraft is saturated and entrains environmental air at a rate equal to that in the updraft.

(iii) θ_{em} is defined following Johnson (1980); the mesoscale downdraft starts at the melting level with $\theta_{em} = \tilde{\theta}_e$, and θ_{em} is constant in the downdraft layer. No mesoscale downdraft is computed if cloud top is not at least 100 mb above the freezing level. Relative humidity r_m follows Leary and Houze (1980), with the following exception:

$$r_m \geq [\bar{r}], \tag{14}$$

where $[\bar{r}]$ is the mean grid scale relative humidity in the downdraft layer. This prevents unrealistically warm and dry mesoscale downdrafts in the presence of a nearly saturated grid-scale environment.

(iv) Both cumulus and mesoscale downdrafts are included in the weighted sum only when they are negatively buoyant. A crude water loading effect is added by allowing a 0.5°C temperature excess in the downdrafts, roughly equivalent to 1.5 g kg^{-1} of liquid water.

(v) In the downdraft layer, θ_{ec}, the weighted mean θ_e, is determined from:

$$\theta_{ec} = \frac{w_u\theta_{eu} + w_d\theta_{ed} + w_m\theta_{em}}{w_u + w_d + w_m}, \tag{15}$$

with an analogous expression for q_c. Above the downdraft layer, $\theta_{ec} = \theta_{eu}$.

(vi) T_c is extracted iteratively from θ_{ec} and q_c.

The θ_e weights are determined by the magnitude of the moist static energy change produced by each component. This quantity cannot be computed with the simple cloud model used here, but rather is determined from observed mean values in the convectively active wave trough region in GATE, following Johnson (1980). If downdraft detrainment is assumed to occur only below cloud base, the eddy

flux convergence in the downdraft layer can be written as:

$$-\frac{\partial}{\partial p}(\overline{\tilde{h}'\tilde{\omega}'}) = \delta(p)[h_u(\lambda_d, p) - \tilde{h}(p)] - (M_u + M_d + M_m)\frac{\partial \tilde{h}}{\partial p}, \quad (16)$$

where

$$h = gz + c_pT + Lq \quad (17)$$

is the moist static energy, $\delta(p)$ is updraft detrainment and M is mass flux. Because only deep cumulus clouds can be modelled by the Kuo approach, Johnson's values are taken only for clouds having their detrainment level above 400 mb, and thus the first term in (16) vanishes, and the weights are determined for each component from its magnitude in the second term (with M_u replaced by M_{uD} in Johnson's data). The weights are shown as a function of pressure in Fig. 1a. Three comments are necessary on this procedure:

(i) The weights are strongly constrained by Johnson's (1980) chosen values for the two parameters: α, the ratio of mesoscale mass flux to updraft mass flux at cloud base, chosen as -0.5 by Johnson; and ϵ, the ratio of cumulus downdraft mass flux at downdraft top to updraft mass flux at cloud base, taken as -0.2. Because Johnson chose these values to best fit the observations, they provide a useful constraint in forming a bulk parameterization of the type considered here.

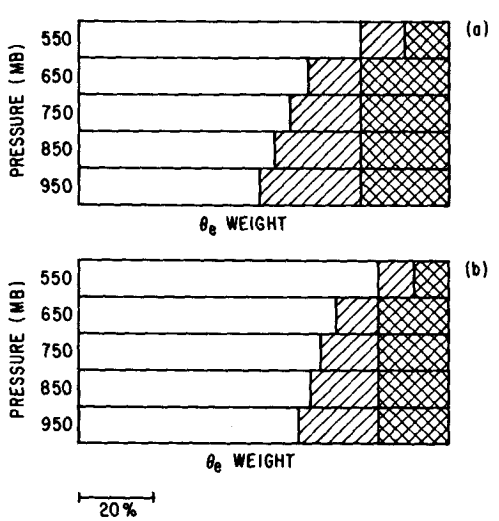

FIG. 1. (a) Relative weights of the θ_e values for updrafts (no shading), cumulus-scale downdrafts (single-line shading), and mesoscale downdrafts (cross-hatching). When the freezing level is nearer 650 than 550 mb, the mesoscale downdraft weighting at the latter level is zero. Values represent absolute weighting in percent when all three components are active at a given level. (b) Altered downdraft weighting used for sensitivity experiments.

(ii) The mean mass fluxes present in the weighting are used solely to determine a mean profile (T_c, q_c) toward which the grid scale will be forced by convection. As in other applications of Kuo's approach, no explicit mass fluxes are computed; only $\bar{\omega}$ is present. By defining the vertical heating profile in this manner, the goal is to force a realistic evolution of the grid-scale ω. A life-cycle behavior in the three-dimensional integration will be discussed in Section 5. Because only T_c and q_c are influenced by the implied mass fluxes, the conservation properties represented by (A9), (A14), and (22) remain satisfied; energy, moisture, and mass are conserved.

(iii) As stabilization occurs and saturation is approached, the three θ_e values come together (Eq. 14 is critical in this), and the ultimate limiting state is moist neutral (if forcing lasts long enough to achieve it). The downdraft formulation thus retains the smooth transition to moist neutrality.

Figure 2 (a, b) shows the overall $T_c - T$ and $q_c - q$ profiles and analogous profiles for the downdrafts alone, for a tropical standard atmosphere sounding (Jordan, 1958). The effect of the ice phase shows in the heating maximum at 350 mb. The downdrafts sharply reduce the heating in the lower troposphere. Cumulus downdrafts are coldest at cloud base, while mesoscale downdrafts are more uniformly cool over a 400 mb layer. The profiles vary significantly depending on the structure of the sounding. For instance, increasing the 550 mb relative humidity by 0.2 reduces the negative buoyancy in the mesoscale downdraft to one-third of that shown, and shifts the cumulus downdraft top to 650 mb. Figure 2 represents the profiles for tropical standard atmosphere only.

4. One-dimensional integrations

The approach will be tested in a one-dimensional framework in which (2)–(3) are integrated from a tropical standard atmosphere initial state. The conditions for invoking the convective calculation follow Molinari (1982b). The vertical motion is specified (Fig. 3) and constant in time. One-dimensional integrations are limited in that ω is not allowed to respond to the heating. Nevertheless, useful information on the relative rate of stabilization of the Kuo approach under various conditions will be obtained.

The apparent heat source Q_1 (Yanai *et al.*, 1973) can be defined for (2)–(3) following Krishnamurti *et al.* (1983):

$$\frac{Q_1}{c_p} = a_\theta\left(\frac{T_c - T}{\Delta\tau} + \omega\frac{T}{\theta}\frac{\partial\theta}{\partial p}\right). \quad (18)$$

Figure 4 shows the apparent heat source for the given ω for the tropical standard atmosphere, with and without downdrafts. As noted in Section 2c, the instantaneous vertically integrated Q_1 is fixed by the

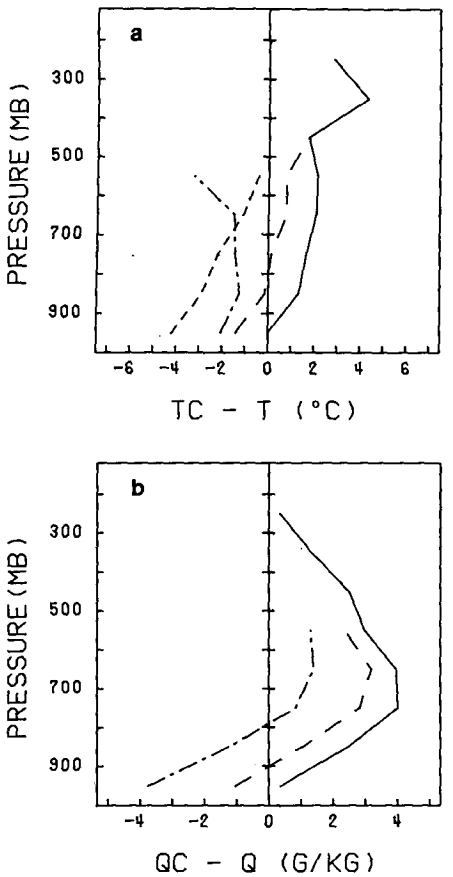

FIG. 2. (a) Temperature difference (°C) between tropical standard atmosphere and the idealized cloud profile without downdrafts (solid), with both downdrafts included (large dash), for mesoscale downdrafts only (dash-dot), and for cumulus downdrafts only (small dash). (b) Specific humidity difference (g/kg) between tropical standard atmosphere and the idealized cloud profile with downdrafts (solid), for cumulus downdrafts only (dashed), and for mesoscale downdrafts only (dash-dot).

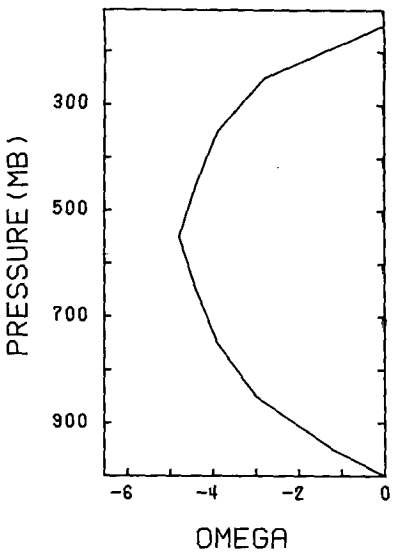

FIG. 3. Vertical motion (μb s^{-1}) specified for the one-dimensional integrations.

choice of b (for a given moisture supply), regardless of T_c and q_c. The major effect of downdrafts on Q_1 is to shift the heating from lower to upper levels. A negative heat source is produced only at the lowest level (950 mb), but mesoscale downdrafts reduce the magnitude of the heating at and below 550 mb, and cumulus downdrafts do the same at and below 750 mb. The Q_1 produced by mesoscale downdrafts alone shown in Fig. 5 (defined by the total Q_1 minus that without mesoscale downdrafts) is similar to that deduced by Houze (1982) from radar data.

Because the rate at which the grid scale approaches stabilization is not specified in Kuo's approach, but rather is variable, it is important to identify the role of various parameters on the stabilization rate. This will be measured by defining the time required for $T_u - T$ (T_u is the entraining updraft temperature), averaged over the cloud layer, to reach 0.25°C from its initial value of 2.01°C in the tropical standard atmosphere, under the steady forcing shown in Fig. 3. Figure 6 shows how this time varies as a function of the b parameter, the presence of downdrafts, the strength of the forcing, the presence of surface fluxes, and the reduced downdraft weighting shown in Fig. 1b. Two sets of experiments are not plotted: those with no downdrafts and those with mesoscale but not cumulus downdrafts. These cases, for all values of b tested, did not reach the 0.25°C limit within 12 hours.

The stabilization characteristics of the Kuo approach with downdrafts can be summarized as follows:

1) As precipitation efficiency $1 - b$ increases, the rate of stabilization increases.

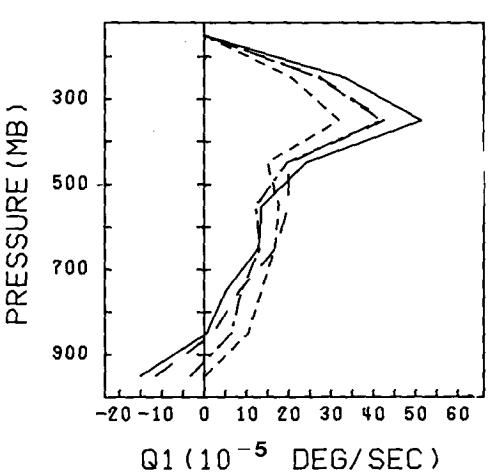

FIG. 4. Apparent heat source (10^{-5} deg s^{-1}) for tropical standard atmosphere under the forcing shown in Fig. 3, without downdrafts in the cloud profile (small dash); with mesoscale downdrafts (dash-dot); with cumulus downdrafts (large dash); and with both downdrafts (solid).

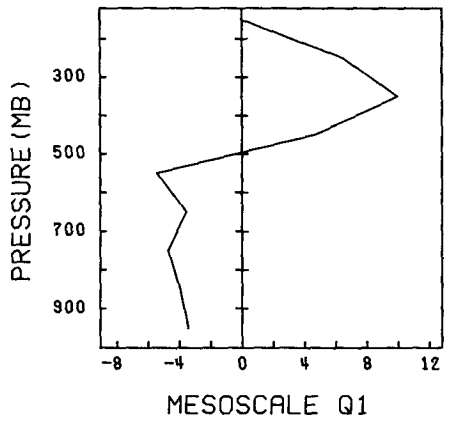

FIG. 5. Apparent heat source (10^{-5} deg s^{-1}) for the mesoscale downdrafts only.

2) Cumulus downdrafts dominate the stabilization process; when they are removed, no integration reaches complete stabilization within 12 hours.

3) Mesoscale downdrafts contribute only slightly; when they are omitted, the stabilization time increases by less than 25%.

4) The Kuo approach always moves the sounding toward a more stable state. The value of $T_u - T$ decreases steadily in all integrations, even those without downdrafts (as shown by Molinari, 1982b). What differs is the rate of stabilization, which increases dramatically when cumulus downdrafts are incorporated.

5) The mesoscale downdraft relative humidity has a significant effect at its extreme value. When mesoscale downdrafts are assumed to be saturated, stabilization takes place more than twice as rapidly for all values of b tested. A realistic unsaturated mesoscale downdraft and separation of cumulus and mesoscale downdrafts is thus necessary in the approach.

6) As the external forcing (measured by the magnitude of the imposed vertical velocity) increases, the rate of stabilization increases.

7) When the θ_e weights are altered to reduce downdraft influence (Fig. 1b), the stabilization time increases significantly.

8) Surface fluxes over relatively warm water reduce the stabilization rate. For the experiments shown, water temperature is assumed to be 302 K, 3°C more than the initial surface air temperature. Heat and moisture fluxes are computed bulk aerodynamically, following Krishnamurti *et al.* (1976), assuming a steady surface wind speed of 10 m s^{-1}. As initial low-level cooling occurs, surface fluxes are enhanced, which slows the decrease of θ_e at cloud base and thus reduces the stabilization rate. Surface heat flux can be even more important in daytime over land, if part of the grid area remains undisturbed and thus heated by the sun.

The internal parameters which have the greatest influence on stabilization rate in the Kuo approach with downdrafts are (a) the b parameter; (b) the updraft/downdraft weighting; and (c) the mesoscale downdraft relative humidity. The first two are chosen from observational studies, and the third relies heavily on observations (Leary and Houze, 1980). Thus, although a variable stabilization rate is allowed, the response of the approach to sensitive parameters is strongly constrained by observed behavior.

5. Three-dimensional integrations

a. Case study

Three-dimensional primitive equation integrations, in which ω responds freely to the heating, provide the most thorough test of the new approach. A real-data prediction is made of the mesoscale convective complex (MCC) described by Bosart and Sanders (1981). This unusually long-lived MCC moved from South Dakota to the Atlantic Ocean between 16 July and 22 July 1977, produced widespread heavy rains, and was responsible for a disastrous flood in Johnstown, Pa. A 12-hour prediction of this system will be made starting from 1200 GMT 19 July and ending three hours prior to the flood event. Extensive rain fell during this period, which was chosen to match

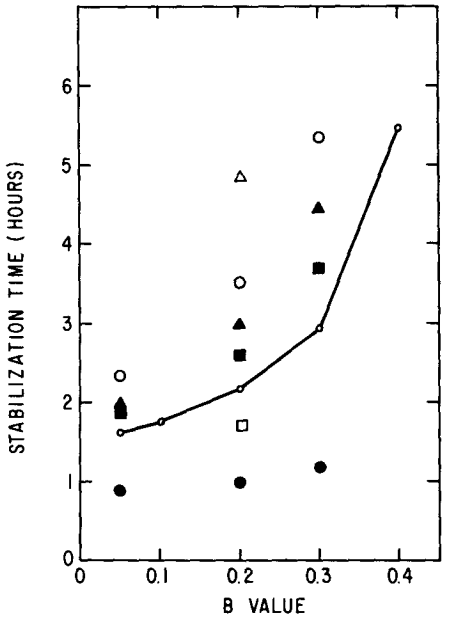

FIG. 6. Time required in the one-dimensional integrations for the entraining updraft temperature excess, averaged over the cloud layer, to drop to 0.25°C, for various values of b, with both downdrafts present (solid line with small open circles); both downdrafts, but saturated mesoscale downdrafts (solid circles); cumulus but no mesoscale downdrafts (solid squares); both downdrafts, with surface fluxes added (solid triangles; see text); using altered downdraft weighting shown in Fig. 1b (open circles); with forcing doubled (open square); and with forcing halved (open triangle).

the availability of subjective analyses of wind, temperature, moisture, and surface pressure kindly provided by Lance Bosart for the initial and verification times, for every 100 mb in the vertical.

The three-dimensional integrations will provide a measure of the ability of a Kuo-type approach to predict the heavy convective precipitation of an MCC. Emphasis will be placed on the importance of downdrafts in the integrations.

b. Model description

The primitive equation model of the author, modified as described below, will be used. The model employs Cartesian coordinates with pressure as the vertical coordinate. The variables are unstaggered in the horizontal and staggered vertically following Molinari (1982a). To prevent separation of solutions in the horizontal on the unstaggered grid, the divergence and pressure gradient are modified following Kanamitsu (1975). Euler-backward differencing is used in time, and the Shuman semi-momentum scheme, in its five-point form (Grammeltvedt, 1969), is used in the horizontal advection terms. All other horizontal derivatives are computed by centered differences. Vertical advection is computed by upstream differencing, following Kanamitsu (1975).

The model equations are as follows.

Momentum equations:

$$\frac{\partial u}{\partial t} = -\mathbf{v}\cdot\nabla_p u - \omega\frac{\partial u}{\partial p} + fv - g\frac{\partial z}{\partial x} - g\frac{\partial F_u}{\partial p} + D_u, \tag{19}$$

$$\frac{\partial v}{\partial t} = -\mathbf{v}\cdot\nabla_p v - \omega\frac{\partial v}{\partial p} - fu - g\frac{\partial z}{\partial y} - g\frac{\partial F_v}{\partial p} + D_v, \tag{20}$$

Hydrostatic equation:

$$\frac{\partial z}{\partial p} = \frac{-RT_v}{pg}, \tag{21}$$

Conservation of mass:

$$\frac{\partial \omega}{\partial p} = -\left(\frac{\partial u}{\partial x} + \frac{\partial v}{\partial y}\right), \tag{22}$$

Thermodynamic equation:

$$\frac{\partial \theta}{\partial t} = -\mathbf{v}\cdot\nabla_p\theta - \omega\frac{\partial \theta}{\partial p} + H_c + H_s + H_R + D_\theta + g\frac{\partial F_H}{\partial p}, \tag{23}$$

Conservation of moisture:

$$\frac{\partial q}{\partial t} = -\mathbf{v}\cdot\nabla_p q - \omega\frac{\partial q}{\partial p} - P_c - P_s + D_q + g\frac{\partial F_q}{\partial p}, \tag{24}$$

Surface tendency equation:

$$\frac{\partial z_0}{\partial t} = -\mathbf{v}\cdot\nabla_p z_0 + \omega_0\frac{R\theta_0}{p_0 g} + \mathbf{v}_0\cdot\nabla h, \tag{25}$$

Definitions:

$$\theta = T(p_0/p)^{R/c_p}, \tag{26}$$

$$T_v = T(1 + 0.61q), \tag{27}$$

where

D represents horizontal diffusion
F represents boundary layer fluxes
H_c is convective heating
H_s is heating due to supersaturation ("stable heating")
H_R is radiative heating
P is net condensation
h is terrain height.

The model is integrated on a 1° latitude–longitude mesh over the region shown in Fig. 8. Lateral boundary conditions are time-dependent and specified entirely from observations, which are linearly interpolated in time over the twelve-hour period. To prevent excessive boundary noise, convective heating is suppressed for grid points adjacent to a lateral boundary. The model has nine vertical levels and a 100 mb vertical resolution.

The model is initialized with observed, subjectively analyzed winds, temperature, moisture and surface pressure. The imposition of balancing (for instance, redefining the mass field via the nonlinear balance equation) may result in a significant loss of information from the analyzed field in the small-scale, highly divergent, convectively driven MCC. Instead, observed winds and mass are used directly and adjust mutually early in the forecast according to primitive equation dynamics and physics. Initial noise damps rapidly, as measured by rms ω values at several levels (Molinari, 1982a). The extensive data base for this case study makes such a procedure feasible.

c. Model physics

Boundary layer momentum fluxes and ocean surface heat and moisture fluxes are computed bulk aerodynamically, following Krishnamurti *et al.* (1976). The bulk aerodynamic approach, though conceptually simple, has been used with success in mesoscale models. Fritsch and Chappell (1980b) simulated convective clusters on the meso-β scale; Anthes *et al.* (1982) accurately predicted a complex interacting set of mesoscale phenomena; and Moss and Jones (1978) simulated many of the observed properties of hurricanes at landfall, all with bulk formulations using a constant drag coefficient over land and another over water. In the current study, $C_D = (0.7 + 0.07*|\mathbf{v}_0|) \times 10^{-3}$ over water (Miller, 1963) and $C_D = 4.3 \times 10^{-3}$ over land (Delsol *et al.*, 1971). The evidence

suggests that this simple approach does not preclude a realistic analysis of the proposed convective parameterization.

Surface moisture flux is neglected over land. Boundary layer radiative heating and cooling and associated heat fluxes over land are determined using the procedure of Fritsch and Chappell (1980b), modified for cloud effects as discussed below. In this procedure the boundary layer sensible heating varies linearly in time from a maximum at 0800 LST to a minimum (maximum cooling rate) at 2000 LST. Because the longitudinal extent of the forecast region is small, heating is assumed, following Fritsch and Chappell (1980b), to be constant with longitude and varying only in time (except for cloud effects). Because the lowest level at which temperature is predicted is 950 mb, the diurnal cycle is applied at that level, with an amplitude of 7.5°C. The resultant heating rate (see Eqs. 12–19 of Fritsch and Chappell, 1980b) is 1.5°C h^{-1} initially (0800 LST), zero at hour 7 (1500 LST), and −1.07°C h^{-1} at hour 12.

The surface boundary conditions on θ and q, needed in the upstream vertical differencing whenever upward motion is present at 950 mb, are determined by the following extrapolation:

$$\theta_{1000} = \theta_{950} - \gamma(\theta_{850} - \theta_{950}), \tag{28}$$

$$q_{1000} = r_{950} q_s(\theta_{1000}), \tag{29}$$

where

$$\gamma = \frac{\bar{\bar{\theta}}_{950} - \bar{\bar{\theta}}_{1000}}{\bar{\bar{\theta}}_{850} - \bar{\bar{\theta}}_{950}},$$

and the double bar indicates an area average over the forecast region. The γ value, computed from the analyzed fields, is 0.638 initially (1200 GMT) and 0.615 twelve hours later. Because γ is nearly identical at differing stages of the diurnal cycle, a single value of 0.626 is assumed to be valid for the entire period. This extrapolation procedure is flexible enough to allow for time variation of stability. As the 950 mb level is heated, for instance, stability is reduced in the 950–850 mb layer, and thus in the boundary layer as well from (28). Figure 7 shows the variation of low-level stability during 12-hour integrations with and without the Fritsch-Chappell heating. The heating and extrapolation procedure produces a reasonable area-averaged diurnal cycle of low-level stability.

In order to compute an approximation for cloud effects, the reduction of insolation produced by cloud decks in the middle and upper troposphere, as might be expected with an MCC, was computed following Katayama (1974) for 0900, 1200 and 1500 LST at the mean latitude and time of year of the model forecast. Shortwave radiative flux reaching the surface was reduced by 60% (±2½%) for the three times. Consequently, cloud effects are incorporated in the model simply by reducing the specified radiative

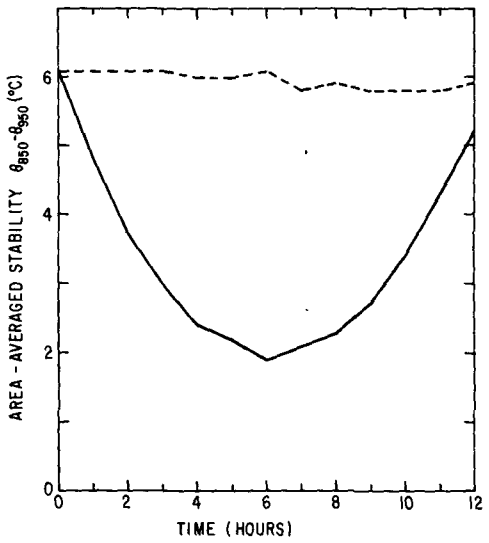

FIG. 7. Time variation of area-averaged low-level stability, measured by potential temperature difference (°C) in the 950–850 mb layer, with the Fritsch-Chappell heating included (solid) and omitted (dashed). Hour 0 is 1200 GMT.

heating by 60% at any grid point in which precipitation is falling during a given time step. The overall procedure is designed to simulate to a first order the diurnal variation of low-level temperature and stability and the reduction of radiative effects by clouds. Cloud-top radiative cooling, which is neglected, is unlikely to be of major significance during the 12 hour integration, which occurs entirely during daylight hours.

The convective parameterization is as described earlier, except that three conditions must be added to account for the many more degrees of freedom in three dimensions. Convection is not invoked, even when other conditions are met, if (a) $A > 0$ (see Eq. A10), which implies that subsidence warming dominates in the column, and convection is suppressed; (b) $Q_\theta < 0$, which implies the updraft has so little buoyancy that negative contributions far exceed positive contributions in $T_c - T$; or (c) $Q_q < 0$, which implies small updraft buoyancy and near-saturation. The latter two conditions prevent a_θ and a_q from becoming negative, which would be physically unrealistic. Condition (c) rarely occurs, but (b) is fairly common for a sounding in which the integrated $T_u - T$ has become nearly zero. At that time, convection is stopped and heating is computed directly from the condensation rate due to supersaturation at each level ("stable heating"). This process employs a relative humidity equation (Kanamitsu, 1975; see Appendix B), which allows calculation of T and q_s during condensation without need of an iterative calculation. The behavior of the approach near neutrality can be seen in the θ_e profiles shown by Molinari (1982b).

d. Results of integrations

The effects of downdrafts on the evolution of the convection and the overall role of convection in the MCC are examined with three integrations: a "full physics" integration which includes both mesoscale and convective scale downdrafts; a second integration identical to the first but with downdrafts removed; and an integration in which no convective heating is allowed, but full physics is present otherwise, including condensation heating produced when saturation is exceeded.

Figure 8 shows the 12-hour rainfall total for the full physics integration, and Fig. 9 (from Bosart and Sanders, 1981) shows the observed rainfall for the same period. A direct comparison is somewhat deceptive, because the observed distribution shows point value amounts, while the predicted gives only grid-area averages. Figure 9 was tabulated on a 0.5° latitude–longitude grid, and mean values were computed over 1° squares. The maximum observed rainfall averaged over a grid area in only 29 mm (in northwest Pennsylvania), comparable to that of the prediction, although a phase error is present. A more quantitative measure is the total volume of rainfall, which was determined by Bosart and Sanders, taking into account the area enclosed by each isopleth. Table 1 shows that the full physics integration predicts the total volume of precipitation over 12 hours from the MCC within 12% of that observed.

Figures 10a–13 show the development of a life cycle at a grid point of heavy precipitation within the MCC. Vertical motion shifted from a middle to upper tropospheric maximum 5–6 hours after the start of the rainfall. During the last hour shown, the rainfall was stratiform only, falling at about 1.5 cm d^{-1} from

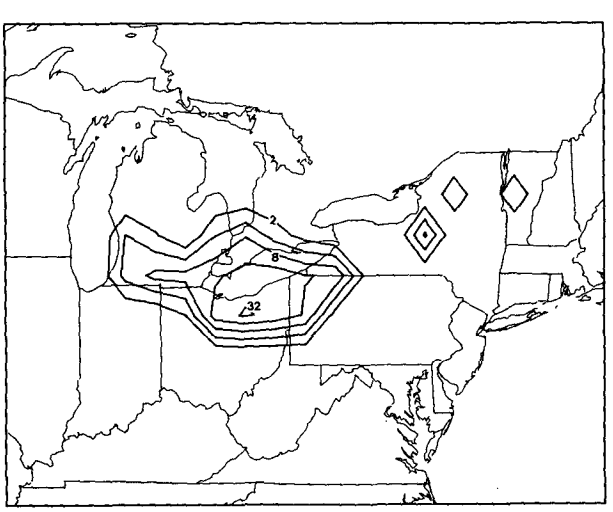

FIG. 8. Total rainfall (mm) over 12 hours for the integration with full physics. Contour increment increases in powers of two, starting from 2 mm.

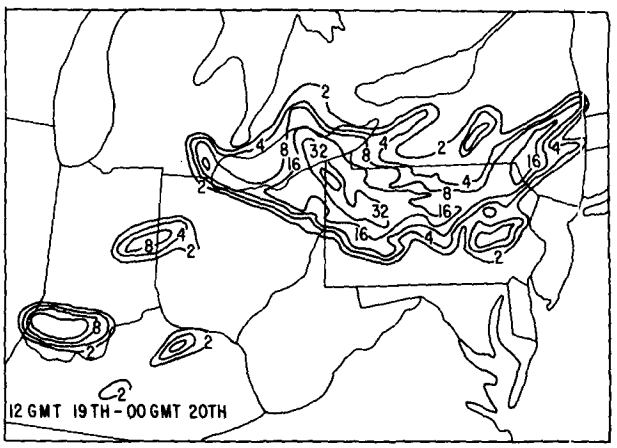

FIG. 9. As in Fig. 8 but for subjectively analyzed observed point-value rainfall amounts (adapted from Bosart and Sanders, 1981).

saturated upper levels, while unsaturated downdrafts were present below (Figs. 10a, 11). The heat source Q_1 at an early time and just prior to the shift to stratiform rain is shown in Fig. 12. The Q_1 values, which include heating due to surface fluxes at 950 mb and are normalized by the rainfall rate, show heating at all levels early in the period, but low-level cooling and relatively greater upper level heating at the later time. In terms of the Kuo approach, the life cycle occurs as follows: precipitation rises rapidly to a peak (Fig. 13), but decays as parameterized downdraft cooling reduces low-level updrafts. Eventually grid-scale downdrafts appear and strengthen until the moisture supply becomes negative (see Eq. 1) and the parameterization is no longer invoked. By this time, the mesoscale updraft/downdraft circulation has developed explicitly on the grid, and stratiform rain falls from upper levels.

When parameterized downdrafts are removed, the behavior is dramatically different (see Fig. 14 and Table 1). At two points, rainfall exceeds 64 mm, and the total volume of rain is overestimated by 28%; the error in rain volume is much larger than when downdrafts are included. Figure 10b shows the time evolution of ω at the same point as earlier. Little or no variation occurs in the lower tropospheric ω, and strong upward motion and intense rainfall (Fig. 13) occur for several hours. This behavior represents a feedback instability that has frequently been experienced in Kuo's approach without downdrafts (e.g., Kanamitsu, 1975). The column is heated, producing upper level divergence, surface pressure falls, a stronger vertical circulation, and more heating. Figure 15 shows the temperature difference at hour 5 between the integrations with and without downdrafts, at a point adjacent to that represented in Fig. 10. The strong low-level cooling by downdrafts represents a 23 K decrease in θ_{es} at cloud base. The corresponding

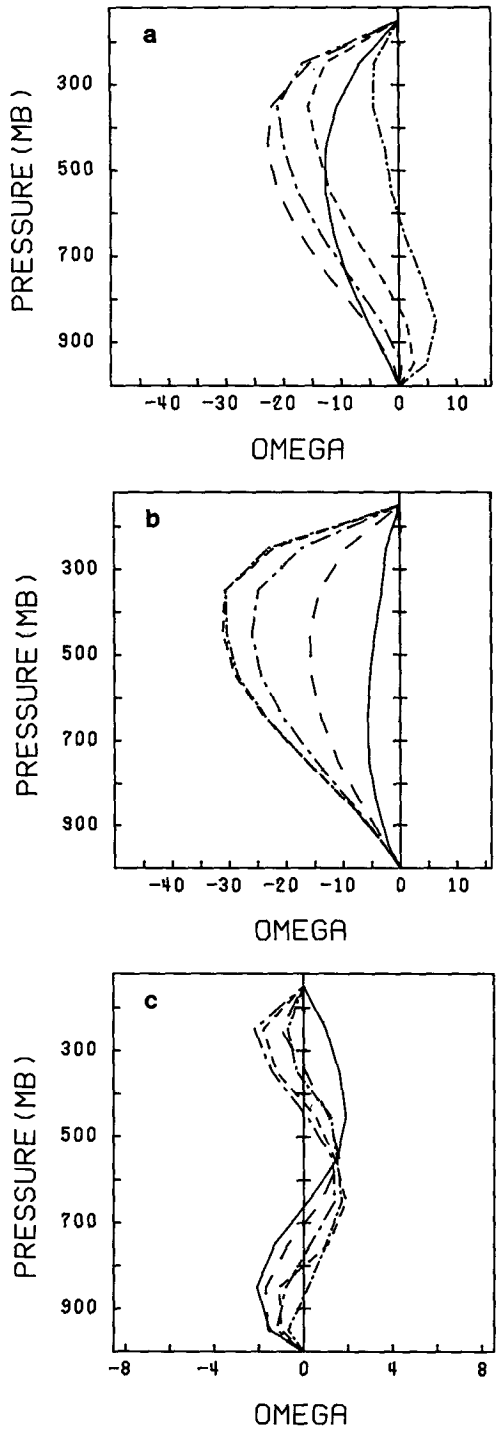

FIG. 10. (a) Vertical motion ($\mu b\ s^{-1}$) for the grid point 10, 6 in the full physics integration at hour 3 (solid), hour 4 (large dash), hour 5 (large dash-dot), hour 6 (small dash), and hour 7 (small dash-dot). (b) As in (a) but in the integration with downdrafts omitted. (c) As in (a) but in the integration without convection.

cooler updraft produces much less warming aloft in the full physics integration. Figures 16–17 show difference fields (no downdraft case minus full physics

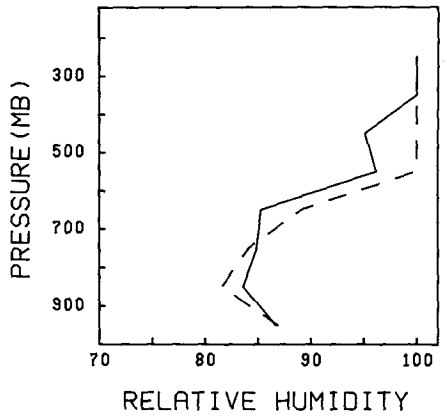

FIG. 11. Relative humidity profile (percent) during the period of upper-level stratiform rainfall at two grid points within the MCC.

case) of 1000 mb height and wind at hour 6. Pressure falls and enhanced low-level convergence accompany the excessive rainfall rates in the integration without downdrafts. The overall effect of downdrafts is to improve the rainfall forecast by incorporating the stabilizing influence of low-level cooling by convection, which greatly reduces the change of the one-grid point instabilities that can otherwise occur.

A third integration with convective heating removed gives a measure of its role in maintaining the MCC circulation. Table 1 shows the dramatic reduction in rainfall in this case. The upward motion generated by model dynamics and physics independent of convection is insufficient to produce widespread saturation and rainfall, and the point value maximum is less than 0.5 cm. The original impulse of upward motion (Fig. 10c), which is generated largely by low-level warm advection (Corsetti, 1982), remains at low levels; no deep vertical circulation ever develops. The role of convective heating can be shown by difference

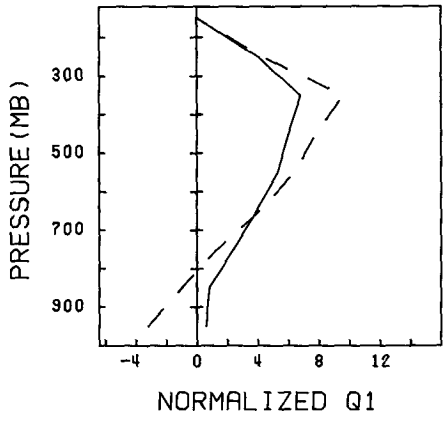

FIG. 12. Apparent heat source, normalized by rainfall rate [units: 10^{-5} deg s^{-1}/(cm d^{-1})], for the full physics integration early in the life cycle (solid) and just prior to the end of convection (dashed). Both convective heating and surface fluxes are included.

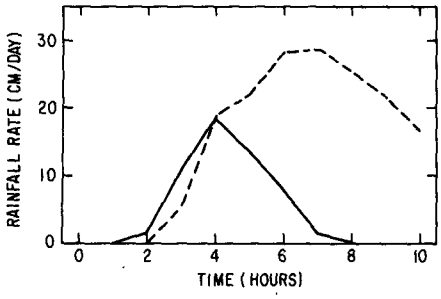

FIG. 13. Time variation of rainfall rate (cm d^{-1}) at the grid point 10, 6 with full physics (solid) and with downdrafts removed (dashed).

vectors between the full physics integration and that without convection. At 200 mb (Fig. 18), strong outflow above the MCC at hour 3 evolves into an anticyclonic eddy which moves with the heavy rainfall region. The outflow, which extends 500 km from the MCC by hour 6 (Fig. 18b), has the same structure as that described in MCC's by Bosart and Sanders (1981), Fritsch and Maddox (1981), and Maddox (1983), and simulated by Maddox *et al.* (1981). The location of the upper anticyclonic eddy in the difference fields at hour 12 is nearly identical to the observed 200 mb anticyclone given by Corsetti (1982). A low-level cyclonic eddy (not shown) develops simultaneously. At 500 mb, the difference vector magnitude is less than 1.5 m s^{-1} everywhere, indicating a much less dramatic influence of convection at mid-levels. The results indicate, not surprisingly, the dominant role of cumulus convection in maintaining an already formed MCC. The question of formation, of course, is entirely separate and cannot be addressed by this study, in which the MCC is already present in the initial state.

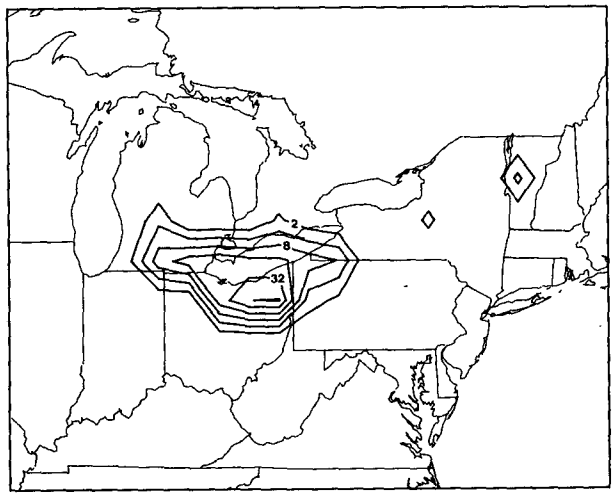

FIG. 14. As in Fig. 8 but for the integration with downdrafts omitted.

TABLE 1. Observed and predicted total rain volume (10^{12} kg) from 1200 GMT 19 July to 0000 GMT 20 July 1977.

	Rain volume	Percent error
Observed	2.15	--
Full Physics	2.41	+12
No downdrafts	2.76	+28
No convection	0.08	−96
Revised b value (Anthes, 1977)	0.57	−74

Because the downdraft weights are derived from GATE data and may not be universal in deep convective situations, the full-physics integration was repeated with the revised weights shown in Fig. 1b. The qualitative behavior of the solution was similar: the life cycle behavior occurred as before, but delayed by one hour; rainfall was 8% larger, but remained less than without downdrafts; and the rainfall pattern was nearly identical. The fundamental conclusions of the paper are not dependent on variation of the downdraft weights within a reasonable range.

A final integration was made to evaluate the influence of a significant change in the b parameter by repeating the full physics integration with b defined following Anthes (1977):

$$b = \frac{1 - \bar{r}}{1 - r_c}, \tag{30}$$

where the bar indicates a vertical average, and $r_c = 0.5$. This definition generally produces a larger b, thus smaller precipitation efficiency, than others (e.g., precipitation efficiency exceeds 70% only when $\bar{r} > 85\%$). Figure 19 shows that rainfall was strongly underpredicted, with the total rain volume (Table 1) less than one third of that observed. This result supports the recent work of Y. H. Kuo (1983), who also found that (30) consistently underestimates the rainfall rate.

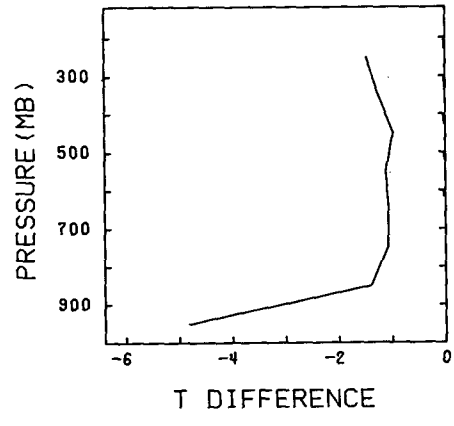

FIG. 15. Temperature difference at the grid point 9, 6 between the full physics and no downdraft integrations at hour 5.

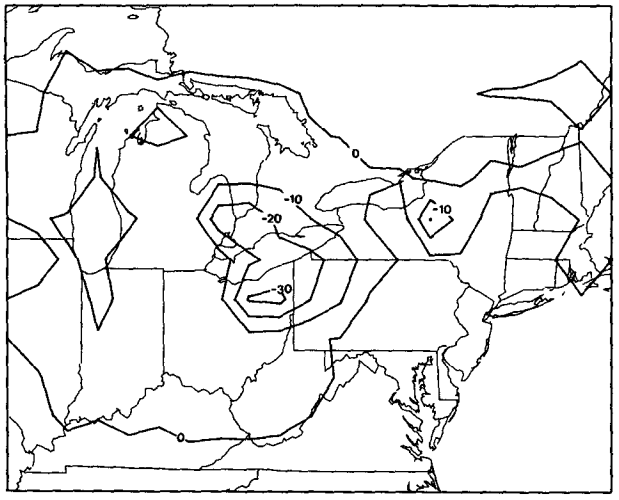

FIG. 16. Difference in 1000 mb height (m) between the no downdraft and full physics integrations at hour 6. Contour interval: 10 m.

6. Discussion and conclusions

Cumulus and mesoscale downdrafts were incorporated into the vertical distributions of heating and moistening in a cumulus parameterization based on the work of Kuo (1974). The addition of downdrafts sharply increased the rate of grid-scale stabilization by the approach. In the prediction of a mesoscale convective complex, only the integration with downdrafts produced an accurate forecast of total rain volume and a realistic life-cycle behavior.

Two potential weaknesses are present in the incorporation of mesoscale processes: (i) mesoscale updrafts are not explicitly considered; and (ii) mesoscale downdrafts are assumed to be present whenever updraft depth and buoyancy criteria are met (see Section 3), and not just in the mature stage of the convective cluster. Uncertainties in the forcing and thermodynamic structure of the mesoscale updraft make it difficult to incorporate in the $T_c - T$ format. Nevertheless, the shift in maximum upward motion to upper levels in the model as the system matured suggests that the updraft heating profile simulated the process described by Johnson and Kriete (1982), in which upper level heating generated midlevel convergence and maintained the mesoscale anvil updraft.

Zipser (1980), in his schematic diagram of a GATE cloud cluster, observed that mesoscale downdrafts do not begin until 2–4 hours after the initiation of deep convective rainfall. Because an MCC was present in

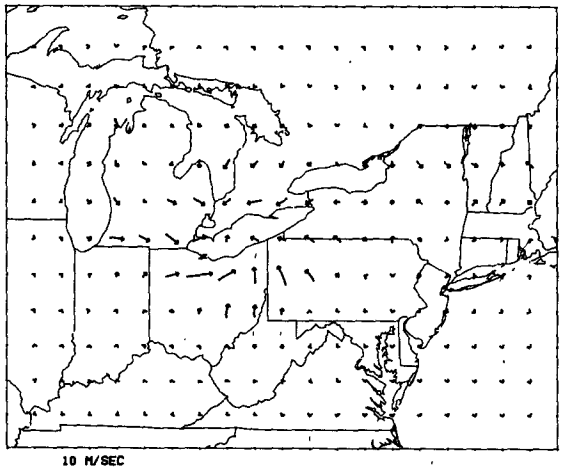

FIG. 17. As in Fig. 16 but for 1000 mb wind vectors.

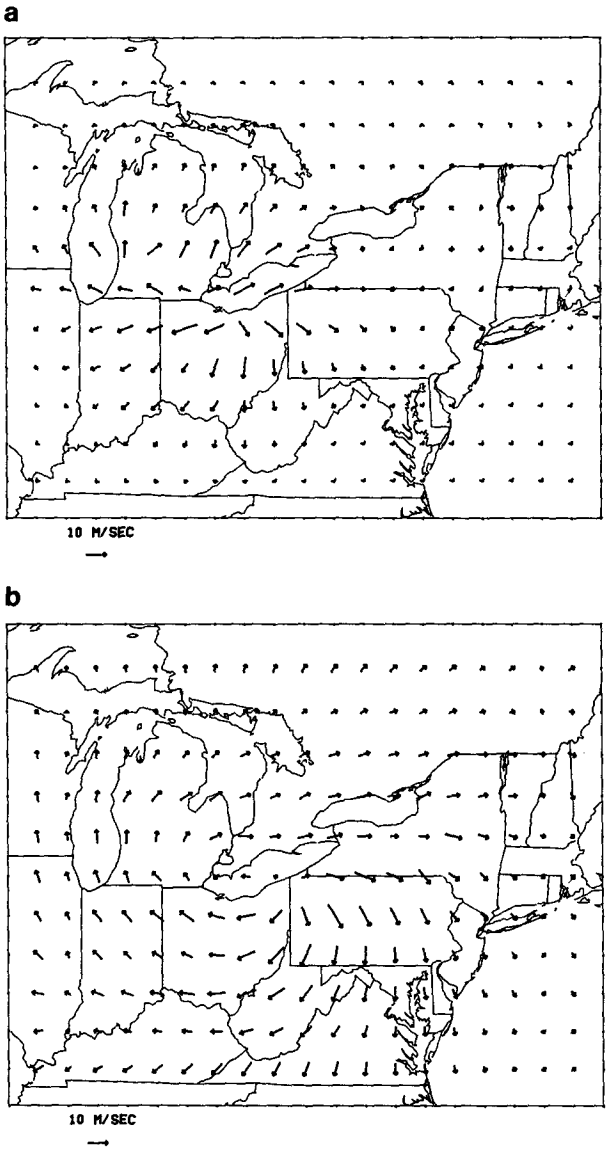

FIG. 18. (a) Difference vectors at 200 mb between the full physics and no convection integrations, at hour 3. (b) As in (a) but for hour 6.

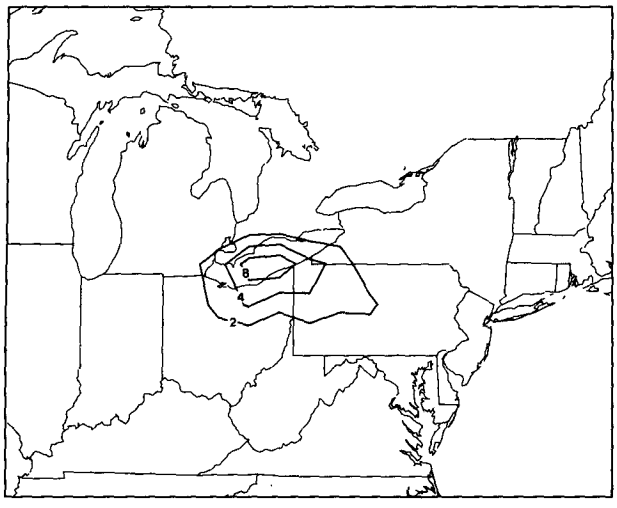

FIG. 19. As in Fig. 8 but for the integration with b defined by Eq. 30.

the initial state in the current study, no attempt was made to build in this lag, although it can be done without violating the integral constraints of the Kuo-Kanamitsu-Krishnamurti approach, by setting $w_m = 0$ for an appropriate period. The occurrence of cumulus downdrafts in nature is also delayed, to a lesser extent. In future experiments, the effects of a lag in the initiation of downdrafts will be investigated.

Orlanski and Ross (1984) have proposed that an explicit calculation of cumulus convection, whereby precipitation occurs only after saturation is reached on the grid scale, is a reasonable substitute for a parameterized approach. That conclusion is not supported by the explicit heating integration in this study, in which a vigorous MCC rapidly decayed and less than 10% of the observed rainfall was generated. It is unlikely that these results would be altered by the 95% saturation criterion of Orlanski and Ross. Although the explicit approach has many advantages for a 10–20 km grid spacing (Rosenthal, 1978), the results of this study indicate it may not be of general value in meso-α scale models, especially when deep convection is active.

Ooyama (1982) and Frank (1983) have noted the difficulty of numerically simulating convectively driven, dynamically small systems (having diameter less than the local Rossby radius of influence), because the divergence field is not a secondary circulation driven by the primary circulation, but instead can interact with the primary system to cause its intensification. The above difficulty is shown in the MCC integrations by the sensitivity of the divergent circulation to the form and distribution of heating: with downdrafts, a large divergent circulation is excited which resembles those described in nature; without downdrafts, the intensity of the vertical circulation is overestimated; and without convective heating, the circulation never develops. Anthes and Keyser (1979) eliminated the rapid spurious intensification of a meso-α scale convective feature by reducing the fraction of heating in the lowest 200 mb by nearly an order of magnitude. Thus, in their study as in this one, the relative magnitude of heating at low levels had a large influence on the interaction of the divergent circulation with the convection.

In this study the convective parameterization simulated many aspects of meso-α scale, convectively driven circulations, as long as downdrafts were incorporated into the limiting state. The detailed examination of cumulus scale-mesoscale interaction cannot be addressed using the current model, in which this interaction must be defined *a priori* by the convection scheme. Nevertheless, the results show that the closure of Kuo, in which the intensity of convection is proportional to the grid-scale moisture supply, may be useful for meso-α scale models.

The limited fine-mesh model of the National Meteorological Center predicted almost none of the observed MCC precipitation, as is frequently the case (Fritsch and Maddox, 1981). In future experiments, an attempt will be made to isolate the role of convective parameterization, versus analysis and resolution limitations, in this failure.

Acknowledgments. The authors thank Lance Bosart for providing detailed subjective analyses of wind, mass and moisture fields for the MCC case, and Richard Johnson for sending printouts of his calculations of the variables used in the θ_e weighting (Johnson, 1980). Comments of an anonymous reviewer improved the organization and clarity of the paper. Acknowledgment is extended to Kathy Stutsrim for her careful typing of the manuscript. This research is supported by National Science Foundation Grant ATM-8317104.

APPENDIX A

Properties of Kuo-Kanamitsu-Krishnamurti Approach

Neglecting nonconvective heating and horizontal advection, equations for potential temperature and specific humidity changes in the presence of convection can be written (Krishnamurti *et al.*, 1976) as:

$$\frac{\partial \theta}{\partial t} = -\omega \frac{\partial \theta}{\partial p} + \left(\frac{p_0}{p}\right)^{R/c_p} \frac{Q_c}{c_p}, \tag{A1}$$

$$\frac{\partial q}{\partial t} = -\omega \frac{\partial q}{\partial p} - C, \tag{A2}$$

where Q_c is the convective heating rate (per unit mass), and C the net drying, due to condensation and eddy fluxes. In both (A1) and (A2), the time change term is the small difference between two large right-hand side terms. In primitive equation models, the vertical motion responds rapidly to the heating field (e.g., see Molinari, 1982a, who imposed 300°C d^{-1} heating in a hurricane simulation), and thus the

θ field remains well-behaved when Q_c is computed separately from the adiabatic cooling term. In the moisture equation, Kuo (1965; 1974) does not calculate the two large, opposing right-hand side terms separately, but parameterizes their sum, which is the net moistening during convection. In this appendix, the Kuo-Kanamitsu-Krishnamurti approach will be reviewed, first without, then with the moisture partitioning of Kuo (1974), and the properties of the approach will be discussed.

To reach cloud temperature T_c in time $\Delta\tau$ requires two components of heating at each level: (i) a warming from grid-scale temperature T to T_c in $\Delta\tau$; and (ii) a warming to balance grid scale adiabatic cooling over $\Delta\tau$. Similarly, moistening is required to increase q to q_c. Because the creation of the cloud represented by T_c and q_c takes place only over a fraction of the area (a), the rate of grid scale heating and moistening needed to form a cloud in $\Delta\tau$ is multiplied by a. Thus

$$\left(\frac{p_0}{p}\right)^{R/c_p}\frac{Q_c}{c_p} = a\left(\frac{\theta_c-\theta}{\Delta\tau}+\omega\frac{\partial\theta}{\partial p}\right), \tag{A3}$$

$$-\omega\frac{\partial q}{\partial p} - C = a\left(\frac{q_c-q}{\Delta\tau}\right). \tag{A4}$$

Kuo (1965) estimated the fraction area by[1]

$$a = I/Q_T, \tag{A5}$$

where I is the rate of moisture accession (defined by Eq. 1 in this work),

$$Q_T = Q_\theta + Q_q \tag{A6}$$

is the rate of moisture accession required to build a cloud in time $\Delta\tau$, and

$$Q_\theta = \frac{1}{g}\int_{p_t}^{p_b}\frac{c_p}{L}\left(\frac{p}{p_0}\right)^{R/c_p}\left(\frac{\theta_c-\theta}{\Delta\tau}+\omega\frac{\partial\theta}{\partial p}\right)dp, \tag{A7}$$

$$Q_q = \frac{1}{g}\int_{p_t}^{p_b}\frac{q_c-q}{\Delta\tau}\,dp. \tag{A8}$$

In the procedure represented by (A1)–(A4), the form of the moisture prediction equation is quite different when convection is active than when $C = 0$. The internal consistency and energy conservation in the approach can be shown by noting that in the absence of convection ($Q_c = C = 0$), (A1)–(A2) can be combined as

$$\frac{1}{g}\int_{p_t}^{p_b}\left(\frac{c_p}{L}\left(\frac{p}{p_0}\right)^{R/c_p}\frac{\partial\theta}{\partial t}+\frac{\partial q}{\partial t}\right)dp = A + I, \tag{A9}$$

where

$$A = -\frac{1}{g}\int_{p_t}^{p_b}\frac{c_p}{L}\left(\frac{p}{p_0}\right)^{R/c_p}\omega\frac{\partial\theta}{\partial p}\,dp \tag{A10}$$

is the vertically integrated adiabatic cooling (in moisture units). In the presence of convection, (A1)–(A2) can be combined using (A3)–(A4) as

$$\frac{1}{g}\int_{p_t}^{p_b}\left(\frac{c_p}{L}\left(\frac{p}{p_0}\right)^{R/c_p}\frac{\partial\theta}{\partial t}+\frac{\partial q}{\partial t}\right)dp = A + \frac{I}{Q_T}(Q_\theta + Q_q) = A + I,$$

and thus (A9) still holds. This reflects the fact that the energy available for convective heating and moistening comes solely from the latent energy supplied to the given grid point.

The approach represented by (A3)–(A4), which uses the same coefficient for heating and moistening, gives a precipitation efficiency of about 0.3 for the tropical standard atmosphere (Kuo, 1965). Because actual precipitation efficiency is much larger, this approach overestimates storage and underestimates precipitation. Kuo (1974) addressed the problem by introducing the parameter b, the fraction of available moisture going into storage; the precipitation efficiency $1 - b$ is thus explicitly present. Kuo (1974) noted that $b \ll 1$, but proposed no functional form. Kanamitsu (1975) and Krishnamurti *et al.* (1976) further developed the approach by defining separate coefficients in (A3) and (A4), and (A1)–(A2) become

$$\frac{\partial\theta}{\partial t} = -\omega\frac{\partial\theta}{\partial p} + a_\theta\left(\frac{\theta_c-\theta}{\Delta\tau}+\omega\frac{\partial\theta}{\partial p}\right), \tag{A11}$$

$$\frac{\partial q}{\partial t} = a_q\left(\frac{q_c-q}{\Delta\tau}\right), \tag{A12}$$

where a_θ and a_q are defined by (4)–(5) in Section 2.

The nature of the b parameter can be seen by vertically integrating (A11)–(A12):

$$\frac{1}{g}\int_{p_t}^{p_b}\frac{c_p}{L}\left(\frac{p}{p_0}\right)^{R/c_p}\frac{\partial\theta}{\partial t}\,dp = A + (1-b)I, \tag{A13}$$

$$\frac{1}{g}\int_{p_t}^{p_b}\frac{\partial q}{\partial t}\,dp = bI. \tag{A14}$$

Equation (A13)–(A14) show that a fraction $1 - b$ of I condenses and opposes adiabatic cooling, while bI goes to moisture storage in the column. Clearly the energy conservation represented by (A9) is still satisfied. Moisture conservation is also insured by defining the precipitation rate as

$$P = \frac{1}{g}\int_{p_t}^{p_b}C\,dp = \frac{1}{g}\int_{p_t}^{p_b}\frac{c_p}{L}\left(\frac{p}{p_0}\right)^{R/c_p}a_\theta\left(\frac{\theta_c-\theta}{\Delta\tau}+\omega\frac{\partial\theta}{\partial p}\right)dp = (1-b)I, \tag{A15}$$

for which (A2), in vertically integrated form, satisfies (A14).

One additional constraint must be satisfied. As a layer reaches moist neutrality ($T \to T_c$, $q \to q_c$, $r \to$

[1] Kuo did not include the adiabatic cooling term in Q_T.

1), the local change of θ and q in (A11)–(A12) must vanish, because both variables are constant for rising motion through a moist neutral layer. This condition insures a smooth transition between unstable and neutral lapse rates. The moist adiabat is defined following Molinari (1982b) as

$$-\frac{\partial\theta}{\partial p}=\frac{L\theta}{c_pT}\frac{\partial q_s}{\partial p}. \tag{A16}$$

As moist neutrality is reached, and if $b \rightarrow 0$ (see Section 2c)

$$I \rightarrow -\frac{1}{g}\int_{p_t}^{p_b}\omega\frac{\partial q_s}{\partial p}\,dp,$$

$$Q_\theta \rightarrow -A,$$

$$a_\theta \rightarrow 1 \quad \text{(using Eq. A16)},$$

$$a_q \rightarrow 0,$$

and from (A11)–(A12),

$$\frac{\partial\theta}{\partial t}\rightarrow 0,$$

$$\frac{\partial q}{\partial t}\rightarrow 0,$$

and thus the current approach satisfies the necessary condition in each layer. As noted by Kanamitsu (1975), the above procedure shows the necessity of including the adiabatic cooling term in (A3) and (A7). In addition, the constraints described in this appendix are valid for any values of T_c, q_c, and b, thus allowing the incorporation of additional physical effects into these variables, as described in Section 3 of the paper.

APPENDIX B

Relative Humidity Equation

The procedure is described in detail by Kanamitsu (1975), and is only briefly reviewed here. The time rate of change of relative humidity (r is actually the saturation ratio q/q_s) can be written

$$\frac{\partial r}{\partial t}=\frac{1}{q_s}\frac{\partial q_s}{\partial t}-\frac{r\epsilon L}{RT\theta}\frac{\partial\theta}{\partial t}, \tag{B1}$$

where $\epsilon = 0.622$, and $\partial q/\partial t$ and $\partial\theta/\partial t$ are from (24) and (23), respectively. They are rewritten here to isolate terms involving condensation due to supersaturation on the grid scale:

$$\frac{\partial q}{\partial t}=\left(\frac{\partial q}{\partial t}\right)_{NS}-P_s, \tag{B2}$$

$$\frac{\partial\theta}{\partial t}=\left(\frac{\partial\theta}{\partial t}\right)_{NS}+H_s, \tag{B3}$$

where subscript NS indicates all terms (including cumulus convection) other than supersaturation heating, and H_s is the heating rate due to condensation P_s, defined by

$$P_s=\frac{c_pT}{L\theta}H_s. \tag{B4}$$

When forcing terms other than supersaturation cause r to exceed one, r must in fact remain at one. Thus H_s is defined using (B1)–(B3) for $\partial r/\partial t = 0$ as

$$H_s=\frac{1}{\dfrac{c_pT}{L\theta q_s}+\dfrac{\epsilon Lr}{RT\theta}}\left\{\frac{1}{q_s}\left(\frac{\partial q}{\partial t}\right)_{NS}-\frac{\epsilon Lr}{RT\theta}\left(\frac{\partial\theta}{\partial t}\right)_{NS}\right\}, \tag{B5}$$

where use has been made of (B4). The heating term H_s is then added to $(\partial\theta/\partial t)_{NS}$ (using Eq. B3) so that after the time step is complete, $r = 1$ and θ includes the effects of stable heating.

In practice, r may be less than one initially, then exceed one during a time step, so that not all of $\partial r/\partial t$ is part of H_s. The general procedure is as follows:

(1) Compute $\partial r^n/\partial t$ without H_s and P_s (superscript n indicates time level). If

$$\frac{\partial r^n}{\partial t}\leqslant\left(\frac{\partial r}{\partial t}\right)_{\text{sat}},$$

where

$$\left(\frac{\partial r}{\partial t}\right)_{\text{sat}}=\frac{1-r^n}{\Delta t} \tag{B6}$$

is the tendency required to saturate in time step Δt, no supersaturation is present, and r^{n+1} and θ^{n+1} are computed directly from (B1) and (B3).

(2) If $\partial r^n/\partial t > (\partial r/\partial t)_{\text{sat}}$,

$$H_s=\frac{1}{\dfrac{c_pT}{L\theta q_s}+\dfrac{\epsilon Lr}{RT\theta}}\left[\frac{\partial r^n}{\partial t}-\left(\frac{\partial r}{\partial t}\right)_{\text{sat}}\right]. \tag{B7}$$

Then $\partial r^n/\partial t$ is set equal to $(\partial r/\partial t)_{\text{sat}}$, i.e., the part of $\partial r/\partial t$ which causes r to reach one is retained, while the remainder is condensed via (B7).

(3) θ^{n+1} is determined from (B3), and q^{n+1} is computed diagnostically from r^{n+1} and θ^{n+1}.

Use of the relative humidity equation allows accurate computation of θ and q during condensation without need of an iterative procedure.

REFERENCES

Anthes, R. A., 1977: Hurricane model experiments with a new cumulus parameterization scheme. *Mon. Wea. Rev.*, **105**, 287–300.

——, and D. Keyser, 1979: Tests of a fine-mesh model over Europe and the United States. *Mon. Wea. Rev.*, **107**, 963–984.

——, Y. H. Kuo, S. G. Benjamin and Y. F. Li, 1982: The evolution of the mesoscale environment of severe local storms: preliminary modeling results. *Mon. Wea. Rev.*, **110,** 1187–1213.

Betts, A. K., 1978: Convection in the tropics. *Meteorology Over the Tropical Oceans,* Roy. Meteor. Soc., Grenville Place, Bracknell, Berkshire, RG12 1BX, England, 105–132.

Bosart, L. F., and F. Sanders, 1981: The Johnstown flood of July 1977: A long-lived convective system. *J. Atmos. Sci.*, **38,** 1616–1642.

Brown, J. M., 1979: Mesoscale unsaturated downdrafts driven by rainfall evaporation: a numerical study. *J. Atmos. Sci.*, **36,** 313–318.

Churchill, D. D., and R. A. Houze Jr., 1984: Development and structure of winter monsoon cloud clusters on 10 December 1978. *J. Atmos. Sci.*, **41,** 933–960.

Corsetti, T., 1982: A numerical simulation of the Johnstown flood of July 1977. M.S. thesis, Dept. Atmos. Sci., State University of New York at Albany, NY, 12222, 76 pp.

Delsol, F., K. Miyakoda and R. H. Clarke, 1971: Parameterized processes in the surface boundary layer of an atmospheric circulation model. *Quart. J. Roy. Meteor. Soc.*, **97,** 181–208.

Frank, W. M., 1979: Individual time period analyses over the GATE ship array. *Mon. Wea. Rev.*, **107,** 1600–1616.

——, 1983: The cumulus parameterization problem. *Mon. Wea. Rev.*, **111,** 1859–1871.

Fritsch, J. M., and C. F. Chappell, 1980a: Numerical prediction of convectively driven mesoscale pressure systems. Part I: convective parameterization. *J. Atmos. Sci.*, **37,** 1722–1733.

——, and ——, 1980b: Numerical prediction of convectively driven mesoscale pressure systems. Part II: mesoscale model. *J. Atmos. Sci.*, **37,** 1734–1762.

——, and R. A. Maddox, 1981: Convectively driven mesoscale weather systems aloft. Part I: observations. *J. Appl. Meteor.*, **20,** 9–19.

Grammeltvedt, A., 1969: A survey of finite difference schemes for the primitive equations for a barotropic fluid. *Mon. Wea. Rev.*, **97,** 384–404.

Hartman, D. L., H. H. Hendon and R. A. Houze Jr., 1984: Some implications of the mesoscale circulations in tropical cloud clusters for large-scale dynamics and climate. *J. Atmos. Sci.*, **41,** 113–121.

Houze, R. A., 1982: Cloud clusters and large-scale vertical motions in the tropics. *J. Meteor. Soc. Japan,* **60,** 396–410.

——, and A. K. Betts, 1981: Convection in GATE. *Rev. Geophy. Space Phys.*, **19,** 541–576.

Johnson, R. H., 1976: The role of convective scale precipitation downdrafts in cumulus and synoptic scale interactions. *J. Atmos. Sci.*, **33,** 1890–1910.

——, 1980: Diagnosis of convective and mesoscale motions during Phase III of GATE. *J. Atmos. Sci.*, **37,** 733–753.

——, and D. C. Kriete, 1982: Thermodynamic and circulation characteristics of winter monsoon tropical mesoscale convection. *Mon. Wea. Rev.*, **110,** 1898–1911.

——, and G. S. Young, 1983: Heat and moisture budgets of tropical mesoscale anvil clouds. *J. Atmos. Sci.*, **40,** 2138–2147.

Jordan, C. L., 1958: Mean soundings for the West Indies area. *J. Meteor.*, **15,** 91–97.

Kanamitsu, M., 1975: On numerical prediction over a global tropical belt. Ph.D. thesis, Dept. of Meteor., Florida State University, Tallahassee, FL 32304, 281 pp.

Katayama, A., 1974: A simplified scheme for computing radiative transfer in the troposphere. Tech. Rep. No. 6, Dept. of Meteor., University of California-Los Angeles, CA 90024.

Krishnamurti, T. N., M. Kanamitsu, R. Godbole, C. B. Chang, F. Carr and J. Chow, 1976: Study of a monsoon depression (II), Dynamical structure. *J. Meteor. Soc. Japan,* **54,** 208–225.

——, Y. Ramanathan, H. L. Pan, R. J. Pasch and J. Molinari, 1980: Cumulus parameterization and rainfall rates I. *Mon. Wea. Rev.*, **108,** 465–472.

——, S. Low-Nam and R. Pasch, 1983: Cumulus parameterization and rainfall rates II. *Mon. Wea. Rev.*, **111,** 815–828.

Kuo, H. L., 1965: On formation and intensification of tropical cyclones through latent heat release by cumulus convection. *J. Atmos. Sci.*, **22,** 40–63.

——, 1974: Further studies of the parameterization of the influence of cumulus convection on large scale flow. *J. Atmos. Sci.*, **31,** 1232–1240.

Kuo, Y.-H., 1983: A diagnostic case study of the effects of deep extratropical convection on the large-scale temperature and moisture structure. Cooperative thesis No. 74, Pennsylvania State University and National Center for Atmospheric Research, P.O. Box 3000, Boulder, CO 80307, 222 pp.

Leary, C. A., and R. A. Houze Jr., 1979: Melting and evaporation of hydrometeors in precipitation from the anvil clouds of deep tropical convection. *J. Atmos. Sci.*, **36,** 669–679.

—— and ——, 1980: The contribution of mesoscale motions to the mass and heat fluxes of an intense tropical convective system. *J. Atmos. Sci.*, **37,** 784–796.

Maddox, R. A., 1983: Large-scale meteorological conditions associated with midlatitude, mesoscale convective complexes. *Mon. Wea. Rev.*, **111,** 1475–1493.

——, R. J. Perkey and J. M. Fritsch, 1981: Evolution of upper tropospheric features during the development of a mesoscale convective complex. *J. Atmos. Sci.*, **38,** 1664–1674.

Miller, B. I., 1963: On the filling of tropical cyclones over land. National Hurricane Research Project No. 66, HRD/AOML, 4301 Rickenbacker Causeway, Miami, FL 33149, 82 pp.

Molinari, J., 1982a: Numerical hurricane prediction using assimilation of remotely-sensed rainfall rates. *Mon. Wea. Rev.*, **110,** 553–571.

——, 1982b: A method for calculating the effects of deep cumulus convection in numerical models. *Mon. Wea. Rev.*, **110,** 1527–1534.

Moss, M. S., and R. W. Jones, 1978: A numerical simulation of hurricane landfall. NOAA Tech. Memo. ERLNHEML-3, HRD/AOML, 4301 Rickenbacker Causeway, Miami, FL 33149, 15 pp.

Ooyama, R. V., 1982: Conceptual evolution of the theory and modeling of the tropical cyclone. *J. Meteor. Soc. Japan,* **60,** 369–379.

Orlanski, I., and B. B. Ross, 1984: The evolution of an observed cold front. Part II: Mesoscale dynamics. *J. Atmos. Sci.*, **41,** 1669–1703.

Rosenthal, S. L., 1978: Numerical simulation of tropical cyclone development with latent heat release by the resolvable scales I: Model description and preliminary results. *J. Atmos. Sci.*, **35,** 258–271.

Yanai, M., S. Esbensen and J. Chu, 1973: Determination of bulk properties of tropical cloud clusters from large-scale heat and moisture budgets. *J. Atmos. Sci.*, **30,** 611–627.

Zipser, E. J., 1969: The role of organized unsaturated convective downdrafts in the structure and rapid decay of an equatorial disturbance. *J. Appl. Meteor.*, **8,** 799–814.

——, 1980: Kinematic and thermodynamic structure of mesoscale systems in GATE. *Proc. Seminar on the Impact of GATE on Large-Scale Numerical Modelling of the Atmosphere and Ocean,* National Academy of Sciences, 2101 Constitution Ave., NW, Washington, D.C. 20418-0001, pp. 91–99.